Targeting endothelium and its dynamic caveolae for tissue-specific transcytosis *in vivo*: A pathway to overcome cell barriers to drug and gene delivery

Deirdre P. McIntosh*†, Xiang-Yang Tan*†, Phil Oh*‡, and Jan E. Schnitzer*‡§

*Department of Pathology, Harvard Medical School, Beth Israel Hospital, Boston, MA 02215; and ‡Sidney Kimmel Cancer Center, San Diego, CA 92121

Communicated by Alan Garen, Yale University, New Haven, CT, December 10, 2001 (received for review October 10, 2001)

Site-directed pharmacodelivery is a desirable but elusive goal. Endothelium and epithelium create formidable barriers to endogenous molecules as well as targeted therapies *in vivo*. Caveolae provide a possible, yet unproven, transcellular pathway to overcome such barriers. By using an antibody- and subfractionation-based strategy, we generated a monoclonal antibody specific for lung caveolae (TX3.833) that targets rat lungs after i.v. injection (up to 89% of dose in 30 min). Unlike control antibodies (nonbinding or to lipid rafts), TX3.833 targets lung caveolae that bud to form free vesicles for selective and quantal transendothelial transport to underlying tissue cells *in vivo*. Rapid sequential transcytosis can occur to the alveolar air space via epithelial caveolae. Conjugation to TX3.833 increases drug delivery to the lung up to 172-fold and achieves rapid, localized bioefficacy. We conclude that: (*i*) molecular heterogeneity of the endothelium and its caveolae permits vascular targeting to achieve theoretical expectations of tissue-specific delivery and bioefficacy; (*ii*) caveolae can mediate selective transcytosis *in vivo*; and (*iii*) targeting caveolae may provide a tissue-specific pathway for overcoming key cell barriers to many drug and gene therapies *in vivo*.

Molecular medicine has discovered many new therapeutic modalities by using state-of-the-art techniques in molecular biology. High through-put, *in vitro* assays that screen for pharmacological actions on the desired cell type are frequently used to design new drugs. Although such agents are certainly justified by their success *in vitro*, they frequently perform much less effectively *in vivo* where the agent must reach its target cells in a tissue in sufficient quantities to be potent while sparing bystander organs (1). Depending on the route of administration, the endothelium and/or epithelium form significant barriers that greatly limit the *in vivo* accessibility of many drugs, antibodies, and gene vectors to their intended target sites of pharmacological action, namely, the cells inside the tissue (1–4). For example, poor tissue penetration has hindered many monoclonal antibodies from reaching their cell-specific antigens to achieve effective tissue- or cell-directed pharmaco-delivery *in vivo* (1, 3–6). Moving the target from the tissue cell surface to the surface of vascular endothelium has theoretical advantages in tissue-specific delivery (7–10). This vascular targeting strategy still requires the identification of a tissue-specific target on endothelium, validation of expected delivery *in vivo* and, to be useful for many therapies, a means by which to enter and even cross the vascular wall for access to underlying tissue cells (7).

The microvascular endothelium in most organs acts as a significant barrier to the free passage of bloodborne molecules and cells to the underlying interstitium and tissue cells (8, 11). Specific transport mechanisms are expected to exist for the transendothelial transport of essential circulating blood macromolecules to the subendothelial space to meet the metabolic needs of the surrounding tissue cells (8). Continuous endothelium contains distinct flask-shaped invaginations in the plasma membrane called caveolae that are open to the luminal blood vessel space where circulating molecules may enter them (12–14). These caveolae may provide a trafficking pathway for macromolecules into and possibly across cells (7, 8, 11–14). Based on morphological studies showing few plasmalemmal vesicles existing free and unattached to other membranes inside the cell, some investigators have concluded that caveolae are not dynamic but rather static structures (15–18). Yet, caveolae can bud from the plasma membrane via a dynamin-mediated, GTP-dependent fission process (19, 20), and they contain key functional docking and fusion proteins (20–24). Whether caveolae can traffic their cargo across cells (transcytosis) remains unproven, primarily because comparative analysis has not been possible by using probes capable of targeting caveolae with high affinity and specificity *in vivo* vs. physically identical, nontargeting control probes. The utility of caveolae in overcoming cell barriers to facilitate efficient pharmacodelivery *in vivo* is unknown. The molecular composition of caveolae, including possible tissue-specific differences, is unknown.

Methods

Antibody Production. Monoclonal antibodies were generated by standard somatic cell hybridization using 100 μg of silica-coated luminal endothelial cell plasma membranes (P) as an immunogen and were screened by ELISA with P adsorbed onto 96-well trays.

***In Vivo* Biodistribution Studies.** IgG was purified by Protein G chromatography (Pierce) and radiolabeled with ^{125}I using Iodogen (25). The rat tail vein was injected with 10 μg of ^{125}I-IgG in 500 μl of rat serum albumin (10 mg/ml). After 30 min, the rats were anesthetized for thoracotomy, blood sampling by cardiac puncture, and organ removal. Tissues were weighed before counting γ radioactivity to determine antibody per g of tissue. In initial studies, ^{51}Cr-labeled red blood cells were injected to determine actual tissue uptake by subtracting tissue blood volumes. For TX3.833, this correction was negligible, and the practice was discontinued.

Antibody-Au Conjugates. A monodispersed solution of colloidal gold (average diameter = 6 nm) (EM Science) was adjusted to pH 9.2 with K_2CO_3 before adding purified IgG and stirring rapidly for 30 min. Polyethylene glycol (M_r 20,000) was added to a concentration of 0.5 mg/ml for the last 5 min. After centrifugation at 105,000 $\times$ *g* for 1 h at 4°C, the loose pellets were collected and resuspended in 5 mM phosphate before dialysis against 50 mM Tris during which NaCl was added slowly to a concentration of 150 mM. The conjugates were used within 48 h of preparation.

Abbreviations: P, silica-coated luminal endothelial cell plasma membranes; EM, electron microscopy; H, tissue homogenates; V, isolated caveolae; TTI, tissue targeting index; dgRA, deglycosylated Ricin A chain; 5′NT, 5′-nucleotidase.

†D.P.M. and X.-Y.T. contributed equally to this work.

§To whom reprint requests should be addressed at: Sidney Kimmel Cancer Center, 10835 Altman Row, San Diego, CA 92121. E-mail: jschnitzer@skcc.org.

The publication costs of this article were defrayed in part by page charge payment. This article must therefore be hereby marked "*advertisement*" in accordance with 18 U.S.C. §1734 solely to indicate this fact.

Tracking Antibody-Au Complexes Perfused *in Situ* and *in Vivo*. For the *in situ* experiments, the cranial lobe of the rat lung was perfused at 10 mmHg with PBS+ (PBS containing 3% BSA and 14 mM glucose) at 37°C followed by 6 ml of TX3.833-Au or control mouse IgG_1-Au in PBS+ (OD_{540} = 18). Pulmonary artery perfusion was limited to the cranial lobe by ligature exclusion of all other lobes of the lung. After 2, 5, 10, or 15 min, the lobe was flushed with 6 ml of PBS+ at 37°C before perfusion fixation with 2% (wt/vol) paraformaldehyde and 2.5% (wt/vol) glutaraldehyde in 0.1 M Na cacodylate (KII). The removed lobe was processed for Epon embedding and electron microscopy (EM) as described in (19). To track TX3.833-Au *in vivo*, a TX3.833-Au (15 nm) conjugate (500 μg Ab) was injected directly into rat tail veins. After 15 min, the rat was given intramuscular anesthesia and, as described above, the lungs were flushed with PBS+ followed by KII and processed for EM (19).

Morphometry. Randomly selected fields were examined and recorded at a final magnification of ×49,500. As described (13, 19), an image analyzer (Analytical Imaging Concepts, Roswell, GA) was used to determine the number of gold particles in caveolae per unit surface of linear plasma membrane (4 μm) and in the interstitium per unit surface area (μm^2) of each compartment. We also quantified the number of gold particles found in >150 well defined, apparently single caveolae (no other connecting caveolae or part of one visible in the section) that were clearly attached to the luminal or abluminal plasma membrane by their necks. To minimize variability from sectioning, only caveolae whose diameter exceeded 50 nm were used.

Immuno-Conjugations. Conjugation of ^{125}I to antibody was performed by using Iodogen (25). Deglycosylated Ricin A chain (dgRA) (Sigma) was radio-iodinated (25), reduced with 5 mM DTT and filtered through a Sephadex G25 (Amersham Pharmacia) column in phosphate-EDTA buffer (pH 7.5). N-succinimidyl-3-(2-pyridyldithio)-propionate (SPDP) and sulfosuccinimidyl 4-(N-maleimidomethyl)cyclohexane-1-carboxylate (SMCC) (Pierce) were used to conjugate dgRA or ^{125}I-dgRA to antibody by disulfide linkage or thioether linkage, respectively (26). The antibody conjugates were protein G affinity-isolated.

Results

Novel Antibody Specific for Lung Caveolae. To identify tissue-specific vascular targets and to address whether caveolae can function in selective transport *in vivo*, we generated mouse monoclonal antibodies to rat lung P and their attached caveolae (22, 27). Our screening identified an IgG_1 monoclonal antibody, TX3.833, that seems to be both tissue- and caveolae-specific. Immunoblotting revealed that TX3.833 specifically recognizes a 90-kDa protein expressed in lung but not in other tissues and enriched in lung P relative to the tissue homogenates (H) (Fig. 1 *A* and *B*, and see Fig. 7, which is published as supporting information on the PNAS web site, www.pnas.org). Further subfractionation of lung P to isolate caveolae (V) showed that this antigen is concentrated in caveolae (Fig. 1*B*) similar to caveolin-1 but unlike the lipid raft marker, 5′nucleotidase (5′NT). Densitometry performed under equal protein loading conditions revealed >15-fold enrichments for this antigen both in P relative to H and in V relative to P (>225-fold in V relative to H; n = 3). TX3.833 antigen also was detected in caveolin-1-coated caveolae isolated from V by using caveolin-1 antibodies (28, and data not shown).

Antibody mapping of P reveals considerable molecular diversity of endothelia among organs with differential expression of transferrin receptor, thrombomodulin, 5′NT, and caveolin-1 (Fig. 1*A*). TX3.833 antigen is only detected in P from lung and not other organs. Rat tissue immunostaining confirmed TX3.833 reactivity in lung alveolar microvasculature but not in bronchial

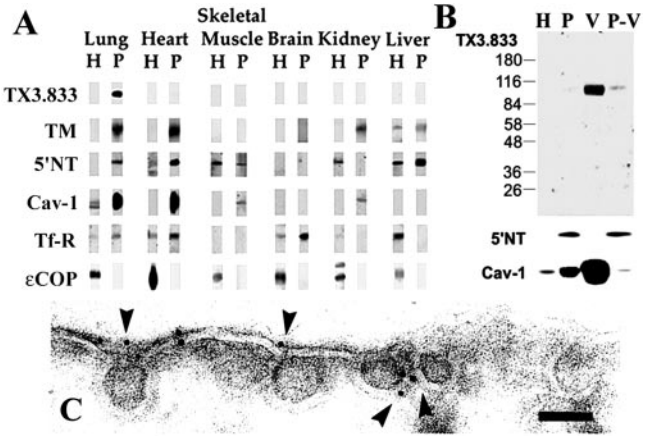

Fig. 1. Characterization of TX3.833. (*A*) Proteins (10 μg each lane) from the indicated H and P were subjected to Western analysis by using antibodies to the indicated proteins as in our past work (22, 27). (*B*) Proteins (5 μg) from rat lung H, P, V, and silica-coated plasma membranes stripped of caveolae (P-V) were immunoblotted by using TX3.833 and monoclonal antibodies to 5′NT and caveolin-1. (*C*) Ultra-thin cryo-sections of rat lung tissue were labeled with TX3.833 followed by reporter antibody conjugated to gold particles and were examined by EM. Arrowheads indicate endothelial caveolae. (Bar = 90 nm.)

epithelium, larger pulmonic vessels, or in any blood vessels of the heart, liver, brain, kidney, intestine, skeletal muscle, testes, spleen, skin, and adrenal (data not shown). More importantly, immunogold EM carried out on ultrathin frozen lung tissue sections showed that TX3.833 associated predominantly with the bulb and necks of the caveolae in microvascular endothelium (Fig. 1*C*, and Fig. 8, which is published as supporting information on the PNAS web site) and not clathrin-coated pits or epithelial cells (including their caveolae). Larger blood vessel endothelium of lung and controls using heart tissue or nonspecific mouse IgG_1 were negative (data not shown). Thus, TX3.833 specifically recognizes a 90-kDa antigen that is expressed selectively in caveolae of microvascular endothelium of lung but not other tissues.

Tissue Targeting *in Vivo*. To assess possible tissue-specific immunotargeting *in vivo*, we injected purified radio-iodinated TX3.833 or control IgG_1 into rat tail veins. Different biodistributions for each antibody were quite apparent 30 min after injection (Fig. 2 *A* and *B*). TX3.833 showed rapid and substantial lung uptake with very little detected in other organs (values less than or equal to control IgG) and very low blood levels (10-fold less than control). Up to 89% with a mean of 75 ± 6.4% of the injected dose of TX3.833 was targeted to the lungs in just 30 min. As in past reports (29), the control IgG remained in the blood with low tissue uptakes; the liver had the most, apparently because of IgG sequestration by F_c receptors. The lung tropism of TX3.833 was specific because unlabeled TX3.833, but not control IgG, inhibited lung accumulation by 89% and increased blood levels by >15-fold (Fig. 2*C*). Other antibodies generated in our screen recognized endothelial cell surface antigens in several tissues and accumulated *in vivo* in multiple tissues (data not shown). The uptake of TX3.833 significantly exceeds past reports describing various targeting probes (peptides and monoclonal antibodies), sometimes requiring up to 1 week to achieve a maximal tissue uptake of 0.2–4% of the injected dose (4, 6, 29–34). Even 24 h after injection, 46% of TX3.833 still remained in the lung.

Calculation of the tissue targeting index (TTI = antibody in tissue per g of tissue per antibody in blood per g of blood) and tissue selectivity index (TSI = TTI for targeting IgG per TTI for control IgG) confirmed lung targeting of TX3.833 with a mean

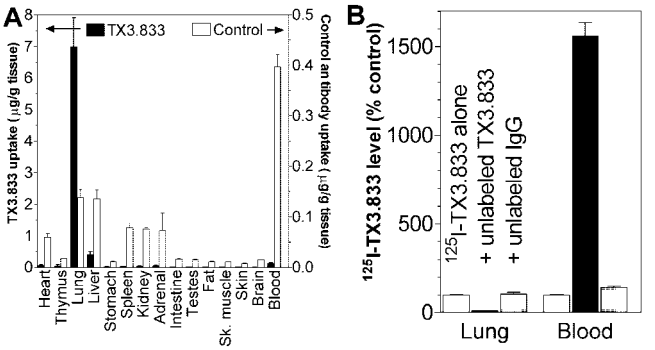

Fig. 2. In vivo biodistribution of TX3.833. (*A*) Blood levels and tissue uptake of ^{125}I-labeled TX3.833 and control IgG_1 (10 μg) were determined 30 min after i.v. injection. The mean value in μg IgG/g of tissue or blood is plotted with SD bars ($n \geq 3$). (*B*) Rats were injected with 1 mg of unlabeled TX3.833 or control IgG 30 min before ^{125}I-TX3.833 (10 μg) and assessed for radioactivity in the lung and blood, which is expressed as a percentage of signal without unlabeled antibody.

TTI of 56 and TSI of 150. The control IgG lacked targeting with TTI < 1 for all organs examined (maximum in liver of 0.36). Last, TX3.833 injections into the right vs. left ventricular chambers produced, even after 15 min, for both injections a TTI >10 for lung and <1 for other tissues. Thus, TX3.833 lung tropism depends not on first pass through the pulmonic circulation but rather on the antigen expression restricted to lung microvascular endothelium.

Transcytosis of Antibody Targeting Lung Caveolae *in Situ*. To assess possible targeting to and transport by caveolae of TX3.833, we perfused TX3.833 conjugated to colloidal gold particles (TX3.833-Au) through the rat pulmonary artery. EM and morphometric analysis (Fig. 3 and Fig. 4) revealed specific and rapid TX3.833-Au targeting to caveolae followed by transendothelial transport of the targeted cargo. Within 2–3 min, TX3.833-Au was found at the endothelial cell surface mostly bound to accessible luminal caveolae, either at their necks (on or near the diaphragm) or penetrating into the bulb of the caveolae (Fig. 3*A*, arrowheads). Very little-to-no TX3.833-Au was detected in caveolae located further inside the cell, attached to the abluminal cell surface, in clathrin-coated pits and vesicles or in the subendothelial space. After 5 min, penetration of TX3.833-Au into the caveolar system increased with many more caveolae containing gold particles including those connected at the luminal surface, further inside the cell, and at the abluminal surface (Fig. 3*B*, arrowheads). Occasionally, gold particles were seen inside (and not yet exiting) abluminal caveolae that opened onto the subendothelial space (data not shown). By 10 min, many gold particles were detected exiting the endothelium from the abluminal caveolae into the subendothelial space (Fig. 3 *C* and *D*, arrows). The amount of gold in the perivascular space was increasing but remained mostly in the proximity of the basal/abluminal endothelial cell plasma membrane (subendothelial space). Gold particles also were observed in racemose caveolar structures (Fig. 3*C*, thick arrow). There was little evidence of caveolae-mediated endocytosis to intracellular organelles such as endosomes (Fig. 3*E*). Although sometimes TX3.833-Au was seen accumulating at a luminal region near endothelial intercellular junction (Fig. 3*E*), little-to-no gold was found in the interstitium at the junctional exit (open arrow), consistent with a lack of transport through this pathway and the expected size-exclusion of the gold particles. After 15 min, TX3.833-Au still was being transported and existed in many luminal, abluminal, and apparently internalized caveolae (Fig. 3*F*, arrowheads). Gold particles continued to accumulate in the interstitium of the tissue (Fig. 3*F*, thick arrows).

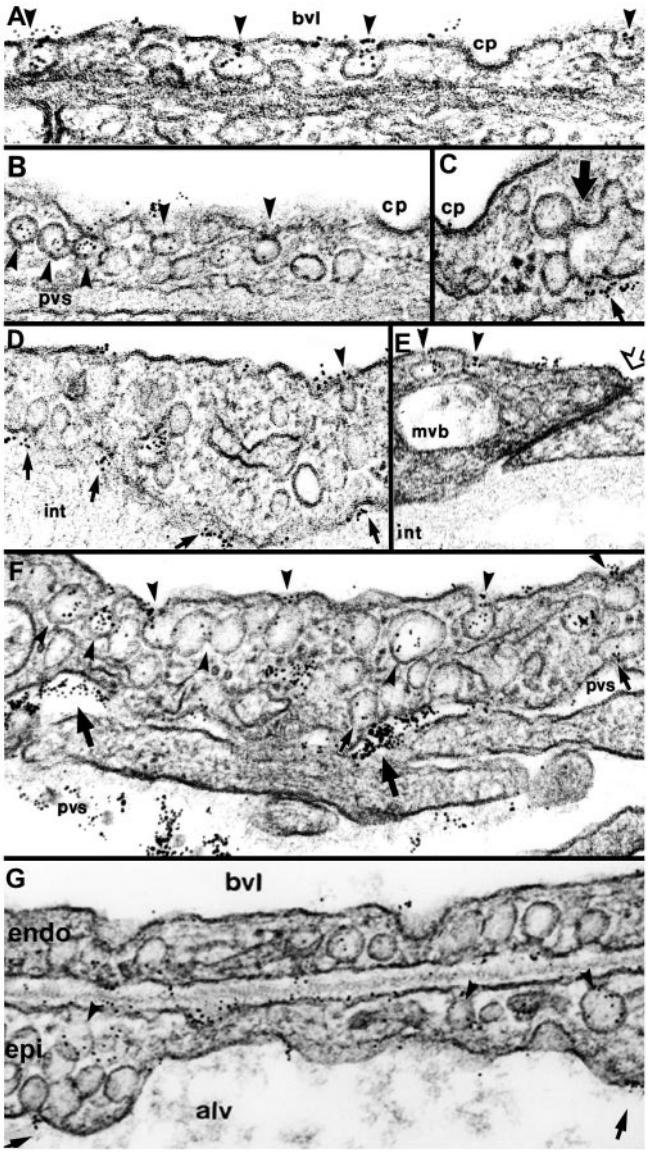

Fig. 3. Caveolar targeting and trafficking of TX3.833-Au *in situ*. The rat lung was perfused *in situ* with TX3.833-Au for 2.5 min (*A*), 5 min (*B*), 10 min (*C–E*), and 15 min (*F* and *G*), and processed for EM. Int, interstitial space; cp, coated pits; bvl, blood vessel lumen; pvs, perivascular space; mvb, multivesicular bodies; endo, endothelium; epi, epithelium; alv, alveolar space. [Bar = 90 nm (*A*), 128 nm (*B*), 116 nm (*C* and *D*), 124 nm (*E*), 90 nm (*F*), 85 nm (*G*).]

In several fortuitous cases, we caught the release of gold particles from the neck or introit of caveola (arrows, Fig. 3 *D* and *F*). The gold particles were seen as a cluster in the region immediately adjacent to the caveolar opening, apparently exiting as a bolus and just beginning to disperse freely into the underlying space. Sometimes one or two gold particles were still found just inside the neck of an otherwise empty abluminal caveola. No other gold particles were seen in the vicinity. Morphometric analysis showed that a similar number of gold particles entered luminal caveolae as exited abluminal caveolae. At 2.5 min, the labeled luminal caveolae clearly attached to the plasma membrane had a mean of 6.4 $\pm$ 0.5 particles per caveola with $<25\%$ of total luminal caveolae exhibiting no labeling or occasionally one or two gold particles. By 10 min, the mean number of gold

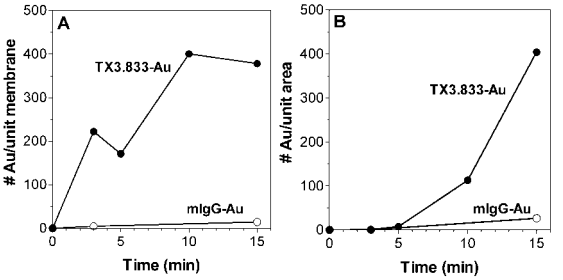

Fig. 4. Analysis of the binding and transport of TX3.833-Au vs. IgG-Au in rat lung. Comparative morphometric analysis was performed on the electron micrographs of rat lungs perfused with TX3.833-Au or mouse IgG-Au (see *Methods*) to quantify over time the number of gold particles (*A*) in lung microvascular endothelial caveolae per unit membrane and (*B*) within the interstitial space per unit area (μm^2).

particles inside labeled luminal and abluminal caveolae was 6.3 ± 0.3 and 7.1 ± 0.6, respectively, although, again, a subpopulation of caveolae (<25%) still had little to no label. Lastly, the mean number of gold particles exiting the neck of abluminal caveola was 6.7 ± 0.8 particles. This quantal uptake, transport, and release of six to seven gold particles per caveolae is consistent with discrete transcytosis of targeted molecular cargo by caveolae.

By comparing TX3.833-Au with physically identical probes having different binding specificity (i.e., all 150-kDa IgG_1 bound in the same way to the same size gold particles), we found that the ability of TX3.833 to specifically target the gold to caveolae mediates its transport across the lung microvascular endothelium. Even after 15 min, control mIgG-Au did not accumulate in caveolae or overcome the endothelial cell barrier (Fig. 9*A*, which is published as supporting information on the PNAS web site). Morphometric analysis showed that both entry to caveolae and interstitial accumulation were significantly more for TX3.833-Au than mIgG-Au (Fig. 4). As an additional control, we tested gold-conjugated antibody to 5′NT (5′NT-IgG-Au), a glycosylphosphatidylinositol-anchored endothelial cell-surface marker concentrated in lipid rafts but not caveolae (22). 5′NT-IgG-Au bound to the lung endothelial cell surface primarily in clusters on the plasmalemma proper that sometimes were at or near the caveolar diaphragm (Fig. 9*B*, arrowhead, which is published as supporting information on the PNAS web site). 5′NT-IgG-Au did not traverse the endothelium to accumulate in the interstitium even after 15 min. Targeting lipid rafts under equivalent conditions did not result in rapid transcytosis. Thus, the TX3.833-Au transported to in the interstitium depended on targeting caveolae.

Sequential Transcytosis. At 15 min with TX3.833-Au, we also found, where the attenuated endothelium was in close apposition to the alveolar epithelium, some of the gold particles accumulating in the subendothelial space percolated through the basement membrane to be taken up by epithelial caveolae for transport into and even across the cell (Fig. 3*G*, arrowhead). Gold particles were sometimes in endosomal-like structures and exiting caveolae opening into the air space (arrow). Although surprising because we detected little TX3.833 antigen in the epithelium by immunogold EM (Fig. 8), it is possible that where the interstitial space separating the endothelium from the epithelium is small enough to allow higher concentration of transcytosed gold particles, the epithelial caveolae could take up and transport the gold particles by fluid-phase mechanisms. Perhaps more likely, the TX3.833 antigen is expressed at lower levels in the epithelial caveolae. Thus, transcellular transport by caveolae occurs not only in endothelium but also in epithelium,

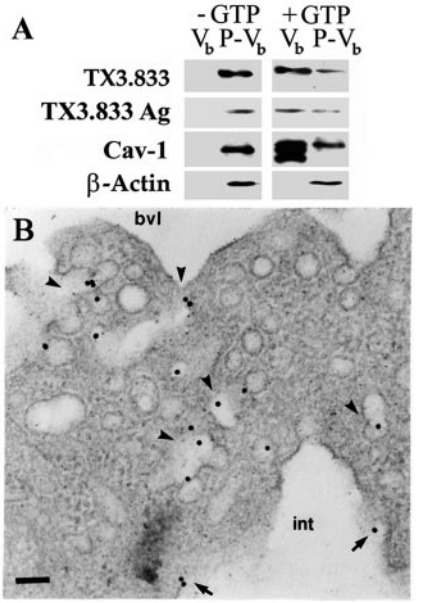

Fig. 5. TX3.833 targets dynamic caveolae *in vivo*. (*A*) Rat lungs were perfused for 5 min with 1 mg of biotinylated TX3.833 before flushing and silica perfusion for isolation of P that was subjected to the caveolae budding assay with or without GTP (20, 22). The budded caveolae (V_b), isolated by flotation away from the repelleted membrane (P-V_b), were immunoblotted with either streptavidin or the indicated antibodies. (*B*) After tail vein injection (15 min), TX3.833-Au is seen selectively in caveolae throughout the endothelial cell, consistent with transcytosis by the caveolae trafficking system. Arrowheads indicate a caveola or group of caveolae with gold particles inside. Arrows show gold particles exiting abluminal caveolae. Bvl, blood vessel lumen; int, interstitial space. (Bar = 91 nm.)

and this sequential transcytosis can be used to overcome rapidly both cell barriers.

TX3.833 Targets Dynamic Caveolae. Some caveolae may be static (15–18). To address whether TX3.833 targets dynamic caveolae capable of budding, we performed a reconstituted budding assay (19, 20) on P from lungs perfused with TX3.833. GTP induced plasmalemmal budding of caveolae that were collected as free floating vesicles containing the injected TX3.833 as well as caveolin-1 and TX3.833 antigen but not β-actin (Fig. 5*A*). This budding required GTP with active dynamin and was inhibited by nonhydrolyzable GTPγS and K44A mutant dynamin (19). Thus, TX3.833 can target dynamic caveolae that require GTP hydrolysis by dynamin for their fission from the plasma membrane to form free transport vesicles.

Tracking Caveolae Targeting and Transcytosis *in Vivo*. Proteins and possibly other elements in the circulating blood increase the restrictiveness of the endothelial cell glycocalyx and can prevent access to caveolae (12). To test the ability of TX3.833 to target lung caveolae *in vivo*, we injected TX3.833-Au into rat tail veins, and 15 min later, we processed the lung tissue for EM. TX3.833-Au could target the lung endothelial caveolae rather selectively (Fig. 5*B*). Gold label could be detected in luminal, abluminal, and apparently cytoplasmic caveolae. Transcytosis was observed with gold particles seen exiting abluminal caveolae to the underlying subendothelial space under normal physiological conditions *in vivo*. This visualization of caveolae targeting and transcytosis *in vivo* was consistent with the antibody-specific targeting of drug shown in Fig. 2 as well as our lung subfractionation analysis showing ^{125}I-TX3.833 (10 min after injection)

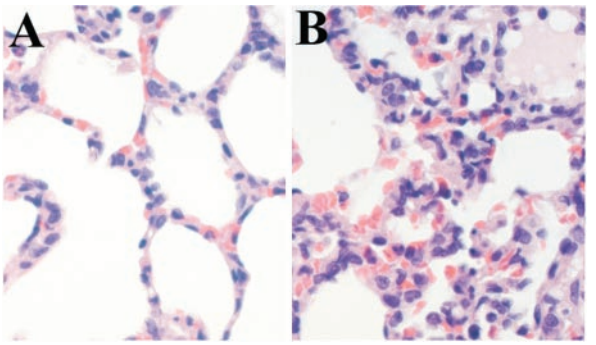

Fig. 6. Drug bio-efficacy studies *in vivo*. Hematoxylin and eosin staining of rat lungs 24 h after treatment with (*A*) control antibody-dgRA or (*B*) TX3.833-dgRA. Note the evident tissue damage with gross change in tissue morphology, infiltration of blood cells into tissue, edema, and septal thickening. (Bar = 1.3 μM.)

was enriched in V at levels 100-fold > ^{125}I-contol IgG (data not shown).

Lung-Specific Delivery and Bioefficacy of TX3.833-Drug Conjugates. An antibody targeting lung caveolae *in vivo* could be useful as a carrier to achieve tissue-specific drug delivery. To test TX3.833 as a targeting vector, we conjugated it to various drugs and examined *in vivo* delivery of the immunoconjugate relative to the native drug. All TX3.833-drug conjugates showed greatly increased lung targeting up to 172-fold greater than drug alone (see Table 1, which is published as supporting information on the PNAS web site). We also examined the bioefficacy of targeted drug by using dgRA immunotoxin, which is highly toxic in small amounts but requires internalization by cells for A chain release into the cytoplasm and subsequent cell death (35). At 6 h after i.v. injection, and even more so at 24 h after, the TX3.833-dgRA-treated rats showed acute respiratory distress and general malaise (very rapid, shallow breathing, remaining stationary, and focused on just breathing). Histological tissue examination revealed lung tissue disruption with edema, blood infiltration, and thickening of septa (Fig. 6) but no detectable damage to any other organs (e.g., see Fig. 10, which is published as supporting information on the PNAS web site). EM also revealed a loss of endothelial junctional integrity, marked membrane vesiculation of both endothelial and epithelial cells, and the presence of surfactant bodies in the alveolar spaces (Fig. 11, which is published as supporting information on the PNAS web site). The rats treated for 24 h with controls (equivalent levels of control IgG-dgRA, unconjugated TX3.833, native dgRA alone, or TX3.833 unconjugated but together with dgRA) appeared clinically and histologically normal (Fig. 10, which is published as supporting information on the PNAS web site). The damage to lung endothelial and epithelial cells is consistent with endothelial transcytosis of TX3.833-Au and uptake by underlying tissue cells. Thus, our cumulative data indicate that directing a drug to endothelial caveolae can provide tissue-specific targeting, transcytosis for access to cells inside the tissue, and localized bioefficacy *in vivo*.

Discussion

The concept of vascular targeting has evolved in the last 20 years from the failure of many directed therapies to reach their intended target tissue cells (4, 7–10). Targeting endothelium because of its inherent i.v. accessibility has potential, but so far requires key "proof of principle" *in vivo*. Although many attempts have been made to identify tissue-specific targets on vascular endothelium and to develop tissue-specific probes for vascular targeting (32, 33), directed delivery *in vivo* has not met theoretical expectations. A lung-targeting monoclonal antibody has been reported, but the antigen is thrombomodulin, which is expressed by many cells, including endothelia of several organs (ref. 32; Fig. 1*A*). Immunotargeting the pan-endothelial marker, PECAM, can improve delivery to the lung (5-fold over control IgG), but only when the antibody is biotinylated and complexed with streptavidin (36). Screening phage display libraries *in vivo* for tissue-homing peptides has provided modest increased tissue delivery (31, 33, 37) with <1% of the injected dose and relative targeting indices of 2- to 35-fold more than control phage and 3- to 80-fold more delivery than to the brain (note the well known blood–brain barrier has, as expected, the least nonspecific binding and uptake). By using this last criteria, TX3.833 targeting index is >1,000-fold more to lung than brain. TX3.833 as a probe has the specificity and affinity as well as the tissue- and cell-selectivity to validate, for the first time, the vascular targeting strategy by achieving theoretical expectations with high-level tissue targeting *in vivo*. More importantly, perhaps, it targets dynamic caveolae to overcome the endothelial cell barrier for access to underlying tissue cells.

Transport Pathway and Mechanism. Our cumulative *in vivo* and *in situ* data show that (*i*) caveolae can contain a tissue-specific endothelial protein, (*ii*) an antibody can selectively and rapidly target and enter caveolae of microvascular endothelium in a specific tissue, and (*iii*) targeting caveolae greatly increases the transendothelial transport and tissue accumulation over control antibodies (TTI $\geq$ 150). Little transport or tissue accumulation is observed with physically similar, isotype-matched control antibodies that differ from TX3.833 in their ability to recognize a specific caveolar antigen. Thus, it is the specific entry and binding within the caveolae and not just binding to the endothelial cell surface or another microdomain, such as lipid rafts, nor fluid-phase uptake by the caveolae that mediate the rapid and selective transendothelial transport of TX3.833-Au. The graded, time-dependent movement of the caveolae-targeting immunoprobes across the cell barrier cannot be explained by a nonspecific transport pathway (i.e., intercellular junctions) and back-filling of the abluminal aspect of a static, branched caveolar system, as logically proposed (18). Although it is now clear from appropriate controls that caveolae can mediate selective transendothelial transport, the exact mechanism for this transcytosis requires further elucidation.

Over the last 4 decades, two distinct but not mutually exclusive mechanisms for transendothelial transport by the caveolar system have been debated without resolution (8, 11, 15, 16, 18, 38–40): (*i*) active vesicular shuttling of dynamic caveolae that bud from the plasma membrane (20) or even from racemose caveolar structures (39) to form free caveolar transport vesicles carrying their molecular cargo across the cell to fuse with the abluminal membrane; and (*ii*) formation of continuous transendothelial channels through the linkage or temporary fusion of luminal and abluminal caveolae (either as a single caveola or as a group of racemose caveolar vesicles) effectively to form a patent large pore (40). The first mechanism moves a discrete packet of molecular cargo across the cell, whereas probes travel through and exit continuous transendothelial channels as a steady stream of molecules (40). TX3.833 moves across the endothelium not as a continuous stream but rather in discrete packets (six to seven gold particles inside each luminal and abluminal caveola as well as exiting from a then-empty abluminal caveola). The simplest trafficking mechanism consistent with the data has caveolae moving their units of molecular cargo only a short distance across the cell as dynamic, discrete vesicular carriers. Caveolae, like various known trafficking vesicles, have their own molecular machinery to mediate vesicle budding, docking, and fusion, including dynamin, vesicle-associated membrane protein-2, *N*-ethylmaleimide-sensitive factor (NSF), and

soluble NSF attachment proteins (19–24). Here, we show TX3.833 targeting of dynamic caveolae requiring dynamin and GTP hydrolysis to bud from the plasma membrane to form free transport vesicles (19, 20) still carrying the TX3.833 cargo (Fig. 5). These data and the quantal transport of TX3.833-Au support a transcytosis model, in which caveolae bud to transport their targeted cargo into and across the cell.

Large clusters of interconnected caveolae forming cavernous, racemose structures, possibly related to vesiculo-vacuolar organelles (41), may transport a minor portion of TX3.833. Dynamin located at caveolar necks (19) may mediate the budding of individual caveolae or even the whole racemose structure, which may explain the 3- to 5-fold greater amounts of gold probes exiting racemose caveolar structures than any single caveola (e.g., see Fig. 3*C* showing a caveolae racemose structure releasing 25 gold particles). Outside the perinuclear region, endothelial cells, especially in capillaries, are very attenuated, with distances between luminal and abluminal plasma membranes less than or equal to two caveolae diameters (0.1 μm). Most transvascular exchange (11) occurs across such regions with high surface area to volume ratios and little room for racemose caveolar structures. We find the transendothelial transport of TX3.833 occurs mostly in these attenuated regions with the single caveolae carrying their targeted cargo a very short distance. This attenuation may not only speed transendothelial transport into the tissue but also benefit recycling of caveolae back to the luminal surface.

Application for Site-Directed Pharmacodelivery. A selective caveolae targeting strategy may be useful for directed therapeutic delivery for the treatment of many diseases. By targeting caveolae at the luminal surface of endothelium in a single tissue, where the caveolae can transport the antibody from the blood directly into the target tissue, we find that antibodies indeed can provide site-directed delivery *in vivo* with tissue accumulations reaching as high as 89% in just 30 min. Much of this lung-specific accumulation is antibody that has crossed the lung endothelial cell barrier by caveolae-targeted transport to become available for uptake by underlying tissue cells. Here, we have visualized this process by EM to show TX3.833 directing gold particles to the lung caveolae for rapid transendothelial transport from the circulating blood into the tissue. Like many drugs and gene vectors, the gold particles, alone or conjugated to control antibodies, do not readily cross the endothelial cell barrier. When conjugated to potential drugs or toxins, drug delivery by TX3.833 was selective to the lung and enhanced by up to 172-fold. TX3.833-dgRA conjugates selectively damaged the lung, primarily through the destruction of the alveolar endothelial and epithelial cells. Thus, an antibody targeting caveolae can be a carrier to provide tissue-specific pharmacodelivery and bioefficacy through overcoming the endothelial cell barrier that normally restricts delivery to the underlying cells of the tissue.

In our quest to study the basic transport function of caveolae in endothelium, we have shown that caveolae indeed can transcytose select cargo in endothelium as well as epithelium. We have produced and characterized a lung-, microvessel-, and caveolae-specific monoclonal antibody that targets the lung *in vivo*. After intravascular administration, TX3.833 rapidly targets dynamic caveolae of the lung microvascular endothelium and is rapidly transported across the cell for release to the interstitial space where it can be taken up by the caveolae of underlying epithelial cells and transported to the alveolar space. As such, caveolae may provide a selective and useful vesicular trafficking pathway not only to endocytose or transcytose select endogenous molecules but also to overcome the once seemingly insurmountable cell barriers to effective site-directed therapeutic delivery *in vivo*. Moreover, proteomic analysis of endothelial cell plasma membranes and their caveolae reveals several tissue-specific proteins that are differentially expressed in normal organs and in various solid tumors (our unpublished data). Thus, a strategy of targeting caveolae of endothelium and epithelium offers exciting possibilities for achieving site-directed drug and gene therapy of various diseases *in vivo*.

We thank Dr. A. J. Milici and H. Stukenbrok for their assistance and confirmation of the immuno-gold localization of TX3.833 to endothelial caveolae in the lung. We thank Lucy A. Carver for writing assistance. This work was supported in part by funds provided by Tobacco Related Disease Research Program Grant 8RT-0152 and in part by National Institutes of Health Grants HL52766 and HL58216 (to J.E.S.).

1. Jain, R. K. (1998) *Nat. Med.* **4,** 655–657.
2. Miller, N. & Vile, R. (1995) *FASEB J.* **9,** 190–199.
3. Thrush, G. R., Lark, L. A., Clinchy, B. C. & Vitetta, E. S. (1996) *Annu. Rev. Immunol.* **14,** 49–71.
4. Tomlinson, E. (1987) *Adv. Drug Delivery Rev.* **1,** 87–198.
5. Dvorak, H. F., Nagy, J. A. & Dvorak, A. M. (1991) *Cancer Cells* **3,** 77–85.
6. Weinstein, J. N. & van Osdol, W. (1992) *Int. J. Immunopharmacol.* **14,** 457–463.
7. Schnitzer, J. E. (1998) *N. Engl. J. Med.* **339,** 472–474.
8. Schnitzer, J. E. (1993) *Trends Cardiovasc. Med.* **3,** 124–130.
9. Denekamp, J. (1984) *Prog. Appl. Microcirc.* **4,** 28–38.
10. Burrows, F. J. & Thorpe, P. E. (1994) *Pharmacol. Ther.* **64,** 155–174.
11. Renkin, E. M. (1985) *J. Appl. Physiol.* **134,** 375–382.
12. Schneeberger, E. E. & Hamelin, M. (1984) *Am. J. Physiol.* **247,** H206–H217.
13. Milici, A. J., Watrous, N. E., Stukenbrok, H. & Palade, G. E. (1987) *J. Cell Biol.* **105,** 2603–2612.
14. Ghitescu, L., Fixman, A., Simionescu, M. & Simionescu, N. (1986) *J. Cell Biol.* **102,** 1304–1311.
15. Severs, N. J. (1988) *J. Cell Sci.* **90,** 341–348.
16. Rippe, B. & Haraldsson, B. (1987) *Acta Physiol. Scand.* **131,** 411–428.
17. Bundgaard, M., Frokjaer-Jensen, J. & Crone, C. (1979) *Proc. Natl. Acad. Sci. USA* **76,** 6439–6442.
18. Bundgaard, M. (1983) *FASEB J.* **42,** 2425–2430.
19. Oh, P., McIntosh, D. P. & Schnitzer, J. E. (1998) *J. Cell Biol.* **141,** 101–114.
20. Schnitzer, J. E., Oh, P. & McIntosh, D. P. (1996) *Science* **274,** 239–242.
21. McIntosh, D. P. & Schnitzer, J. E. (1999) *Am. J. Physiol.* **277,** H2222–H2232.
22. Schnitzer, J. E., McIntosh, D. P., Dvorak, A. M., Liu, J. & Oh, P. (1995) *Science* **269,** 1435–1439.
23. Schnitzer, J. E., Liu, J. & Oh, P. (1995) *J. Biol. Chem.* **270,** 14399–14404.
24. Schnitzer, J. E., Oh, P., Pinney, E. & Allard, J. (1995) *Am. J. Physiol.* **37,** H48–H55.
25. Fraker, P. J. & Speck, J. C. (1978) *Biochem. Biophys. Res. Commun.* **80,** 849–857.
26. Cumber, A. J., Forrester, J. A., Foxwell, B. M. J., Ross, W. C. & Thorpe, P. E. (1985) *Methods Enzymol.* **112,** 207–225.
27. Oh, P. & Schnitzer, J. E. (1998) in *Cell Biology: A Laboratory Handbook*, ed. Celis, J. (Academic, Orlando, FL), Vol. 2**,** pp. 34–36.
28. Oh, P. & Schnitzer, J. E. (1999) *J. Biol. Chem.* **274,** 23144–23154.
29. Holton, O. D., Black, C. D. V., Parker, R. J., Covell, D. G., Barbet, J., Sieber, S. M., Talley, M. J. & Weinstein, J. N. (1987) *J. Immunol.* **139,** 3041–3049.
30. Pimm, M. V. & Baldwin, R. W. (1984) *Eur. J. Clin. Oncol.* **20,** 515–524.
31. Arap, W., Pasqualini, R. & Ruoslahti, E. (1998) *Science* **279,** 377–380.
32. Hughes, B. J., Kennel, S. K., Lee, R. & Huang, L. (1989) *Cancer Res.* **49,** 6214–6220.
33. Pasqualini, R. & Ruoslahti, E. (1996) *Nature (London)* **380,** 364–366.
34. Christofidou-Solomidou, M., Pietra, G. G., Solomides, C. C., Arguiris, E., Harshaw, D., Fitzgerald, G. A., Albelda, S. M. & Muzykantov, V. R. (2000) *Am. J. Physiol. Lung Cell Mol. Physiol.* **278,** L794–L805.
35. McIntosh, D. P., Edwards, D. C., Cumber, A. J., Parnell, G. D., Dean, C. J., Ross, W. C. J. & Forrester, J. A. (1983) *FEBS Lett.* **164,** 17–20.
36. Muzykantov, V. R., Christofidou-Solomidou, M., Balyasnikova, I., Harshaw, D. W., Schultz, L., Fisher, A. B. & Albelda, S. M. (1999) *Proc. Natl. Acad. Sci. USA* **96,** 2379–2384.
37. Rajotte, D., Arap, W., Hagedorn, M., Koivunen, E., Pasqualini, R. & Ruoslahti, E. (1998) *J. Clin. Invest.* **102,** 430–437.
38. Schnitzer, J. E. (1997) in *Vascular Endothelium: Physiology, Pathology and Therapeutic Opportunities*, eds. Born, G. V. R. & Schwartz, C. J. (Schattauer, Stuttgart), pp. 77–95.
39. Michel, C. C. (1992) *Am. Rev. Respir. Dis.* **146,** S32–S36.
40. Wagner, R. C. & Chen, S.-C. *(1991) Microvasc. Res.* **42,** 139–150.
41. Feng, D., Nagy, J. A., Hipp, J., Dvorak, H. F. & Dvorak, A. M. (1996) *J. Exp. Med.* **183,** 1981–1986.